RECOMMENDATION ITU-R SA.1345

METHODS FOR PREDICTING RADIATION PATTERNS OF LARGE ANTENNAS USED FOR SPACE RESEARCH AND RADIO ASTRONOMY

(Question ITU-R 127/7)

(1998)

The ITU Radiocommunication Assembly,

considering

a) that in many cases reflector antennas used by space research and radio astronomy are similar in that they are of large diameter and operate at frequencies up to tens of GHz;

b) that because of the large distances required to achieve conventional far-field conditions ($2D^2/\lambda$), standard antenna test range or anechoic chamber measurements are inappropriate;

c) that many potential sources of terrestrial based interference to the two services will be in the near-field of the antenna;

d) that accurate models and associated software are becoming available for the prediction of antenna radiation patterns in both the near-field and the far-field, and also for situations which involve interaction with additional reflectors or undesirable obstacles;

e) that the predictions generated by such procedures can in some instances be validated by calibrated measurements,

recommends

1 that where a choice of the most appropriate modelling technique is required for predicting the gain pattern of large reflector antennas, the methods described in Annex 1 and summarized in Table 1 be used:

2 that with respect to modelling techniques involving measurement, the description of the methods in Annex 2 be used as a guide in selecting the most appropriate method;

3 that in determination of the significance of the mechanical characteristics of the antenna to be modelled, attention be paid to the conclusions from the results of computer modelling described in Annex 3.

TABLE 1

Analysis Techniques for Large Reflectors

Sector (see Fig. 1)	Recommended Analysis Techniques
SECTOR I Forward axial sector	Physical Optics
SECTOR II Far sidelobes	Geometrical Theory of Diffraction/Uniform Theory of Diffraction and Induced Field Ratio
SECTOR III Backlobes	Geometrical Theory of Diffraction/Uniform Theory of Diffraction
SECTOR IV Rear axial sector	Equivalent edge currents

FIGURE 1

Sectors for reflector analysis

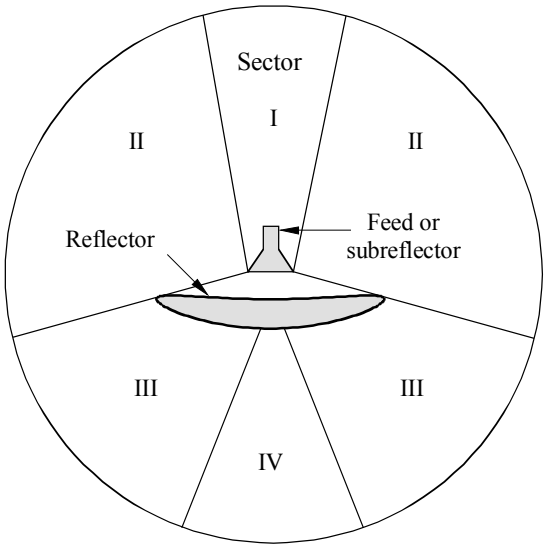

ANNEX 1

Suitability of various electromagnetic modelling methods to predict the gain and radiation patterns of large reflector antennas

1 Introduction

There are a large number of techniques available for solving electromagnetic problems. Each technique may have advantages for modelling particular problems but may be impracticable for other problems. This annex considers the techniques used for the modelling of reflector antennas and considers their suitability for analysis of the large reflector antennas typically used for space research and radio astronomy.

2 Analytical and numerical methods

2.1 Method of moments

The method of moments is a mathematical technique for solving inhomogeneous linear equations of the type:

$$Lf = \mathrm{g} \tag{1}$$

where L is usually a linear integro-differential operator, and the functions f and g are elements of Hilbert spaces. In this equation, g is known and the idea is to invert L to obtain the unknown function $f = L^{-1}g$. The procedure involves a technique that transforms the operator equation (1) to a system of linear algebraic equations. To this end, the unknown function f is expanded in a series of basis functions $\{f_n\}$ with unknown constant coefficients $\{C_n\}$. Substituting this back into equation (1), and taking the inner product of both sides with a set of known testing functions $\{w_m\}$ reduces equation (1) to a simple matrix equation of the form:

$$\mathbf{Ax} = \mathbf{b} \tag{2}$$

where **A** and **b** are given by the inner products $A_{mn} = \langle w_m, Lf_n \rangle$, $b_m = \langle w_m, g \rangle$, and **x** is the vector of unknown coefficients $\{C_n\}$. Equation (2) is easily solved for **x** using elementary numerical methods which then yields f.

In order to apply this technique to reflector analysis, it is necessary to formulate the problem in the form of equation (1). This is accomplished by expressing the field scattered by the antenna as an integral of the unknown surface currents on the reflecting surface. Invoking the electromagnetic boundary condition that the tangential component of the total electric field be zero on a perfect conductor yields an equation for the unknown surface current density $\mathbf{J}_S$ in the form of equation (1) above:

$$\mathbf{u}_n \times \int_S \mathbf{J}_S \bullet \left(\nabla\nabla + k^2 \tilde{\mathbf{I}}\right) G \, \mathrm{d}S = -j\omega\varepsilon_0 \mathbf{u}_n \times \mathbf{E}^i \tag{3a}$$

which is a Fredholm integral equation of the first kind. Here, $\mathbf{u}_n$ is the unit normal to the surface, $\tilde{\mathbf{I}}$ is the unit dyadic given by $\tilde{\mathbf{I}} = \mathbf{u}_x\mathbf{u}_x + \mathbf{u}_y\mathbf{u}_y + \mathbf{u}_z\mathbf{u}_z$, G is the free space scalar Green's function, given by $G = \dfrac{\mathrm{e}^{-jk|r-r'|}}{4\pi|r-r'|}$ with r' and r distances for the source and observation points respectively. $\mathbf{E}^i$ is the incident electric field, and $k = 2\pi/\lambda_0$ is the free space wave number. Equation (3a) can be solved by dividing the surface into small patches over each of which $\mathbf{J}_S$ is expanded as a sum of current components along two orthogonal directions. Alternatively, the reflector may be modelled in the form of a wire grid. This has the advantage that the scattered field can then be expressed as a one dimensional integral of current flowing along the wire. For the case of a thin wire segment along the z-direction defined by the unit vector $\mathbf{u}_z$, the appropriate equation of the form (1) can be given by:

$$j\omega\mu_0 \int \left[I(z) + \left(1/k^2\right) I'(z)(\mathbf{u}_z \bullet \nabla)\right] G \, \mathrm{d}z = \mathbf{u}_z \bullet \mathbf{E}^i \tag{3b}$$

where the prime denotes the derivative. Equation (3b) is solved for the unknown current distribution by expanding it in a suitable set of basis functions.

In principle, this is the most accurate of all known methods used in electromagnetic scattering analysis. The formulation of the governing equation is exact, and extremely accurate solutions can be obtained by a suitable choice of basis and testing functions. In addition, struts, feed, subreflector and supporting structures can all be integrated into the problem. Well-defined surface irregularities on the reflector can be similarly modelled. The technique essentially fragments the complete structure into tiny linear or planar segments, on each of which a boundary condition directly derived from Maxwell's equations is applied by brute force. This results in a coupled system of equations in which electromagnetic interaction of every segment with every other segment is automatically accounted for. The method is, therefore, capable of predicting the complete antenna pattern at all points in space, taking into account the effect of antenna support and related sub-systems. Herein lies the difficulty: assuming a wire grid solution, if the reflector is modelled with M wire segments, and the current in each is represented by N basis functions, this would, in general, lead to a system of MN linear equations in as many unknowns, requiring the numerical evaluation of $(MN)^2$ integrals to obtain the elements of the coefficient matrix. Typically, ten to twenty segments per wavelength with three basis functions per segment are needed for an accurate representation of the currents, leading to a system with over 650 unknowns per square wavelength of the reflecting surface.

In practice, however, some simplifications can be effected. In the case of focus-fed axi-symmetric reflectors, circular symmetry can be exploited to significantly reduce the number of unknown coefficients. In addition, Kirchoff's current law can be invoked at wire junctions to relate some of the unknown constants. In Numerical Electromagnetics Code (NEC), a well-known commercially available suite of moment method software that uses equation (3b), the current $I(z)$ in each segment is represented as the sum of three terms - a constant, a sine and a cosine. Of the three coefficients, two are eliminated by the conditions that charge and current be continuous at wire junctions leaving only one constant, which determines the current amplitude, to be determined by matrix methods. For this representation to be adequate, the length of each wire segment needs to be less than $\lambda/10$, producing over 220 segments per square wavelength of the reflecting surface.

For a 100λ diameter reflector, in the absence of symmetry, this method would require determination of about 1.8 million elements in the coefficient matrix **A**, followed by the inversion of a $1\,340 \times 1\,340$ complex matrix. If the sub-systems and support structures are also modelled, it would result in a significantly larger system of equations. Apart from CPU time, computer memory resources also increase rapidly with reflector size. The method is, therefore, computationally intensive, and is not a viable technique for electrically large reflectors. Typical maximum size for which the method of moments can be successfully applied is 10λ. If circular symmetry is exploited, reflectors as large as 25λ may be analysed. These limits are continuously extended with powerful computer machines becoming available but it is doubtful whether they can be applied to large reflector antennas, at least in the near future.

2.2 Aperture field method

The aperture field method is based on a theorem which states that if S is a closed surface enclosing a finite collection of sources Σ, then the field due to Σ at any arbitrary point exterior to S can be expressed in terms of integrals of field vectors $\mathbf{E}_a$ and $\mathbf{H}_a$ over S, where the subscript a refers to the tangential component. Thus, if S is chosen to be a sphere enclosing the antenna, then a spherical near-field scanning set-up can be used to measure the magnitude and phase of $\mathbf{E}_a$ and $\mathbf{H}_a$ over S, and from this the field of the antenna at every point in space outside S can be computed. However, measuring the near-field over a complete spherical surface surrounding a large reflector is very difficult, if not impossible, to carry out in practice. An alternative is to determine the fields over S by analytical techniques, but with complex sub-systems this is often an intractable problem and various approximations need to be invoked.

One such approximation, called the aperture field method (see Fig. 2a), is based on the assumption that $\mathbf{E}_a$ and $\mathbf{H}_a$ are non-zero over only a finite sector of S. This is justified in the case of a large class of focus-fed convex reflectors where there exists a finite closed contour Γ_A which circumscribes the family of all specularly reflected rays from the illuminated side of the reflector. The projection along the reflected ray paths on S defines a sector $A \in S$, bounded by Γ_A, over which $\mathbf{E}_a$ and $\mathbf{H}_a$ are computed using the laws of geometrical optics, with $\mathbf{E}_a = 0$ and $\mathbf{H}_a = 0$ over $S - A$. This prescription specifies a sharp discontinuity along Γ_A which is inconsistent with Maxwell's equations. To overcome this difficulty, electric and magnetic charge densities are postulated along Γ_A in accordance with the equation of continuity. With this, the field scattered by the reflector is given by the expression:

$$\mathbf{E}_s = \int_A \left[-j\omega\mu(\mathbf{u}_n \times \mathbf{H}_a) - j(\omega\varepsilon)^{-1}(\mathbf{u}_n \times \mathbf{H}_a) \bullet \nabla\nabla + (\mathbf{u}_n \times \mathbf{E}_a) \times \nabla \right] G \, dS \qquad (4)$$

where $\mathbf{u}_n$ is the outward unit normal to A, and G is the free-space scalar Green's function.

Equation (4) forms the fundamental result of the aperture field method, and applies equally to both near- and far-fields exterior to S. In the far-field sector of the antenna, some simplifications can be effected in equation (4) which significantly eases its computational complexity. Its main drawback, however, is the discontinuity postulated along Γ_A which is then overcome by a purely artificial construct. Apart from making the formula consistent with Maxwell's quations, the addition of electric and magnetic charge densities along Γ_A does not make it any more accurate. In actual usage, however, equation (4) is often reduced to a scalar integral by a suitable choice of S, as discussed in the next section. It is in this form that the method is better known.

FIGURE 2

The aperture field method

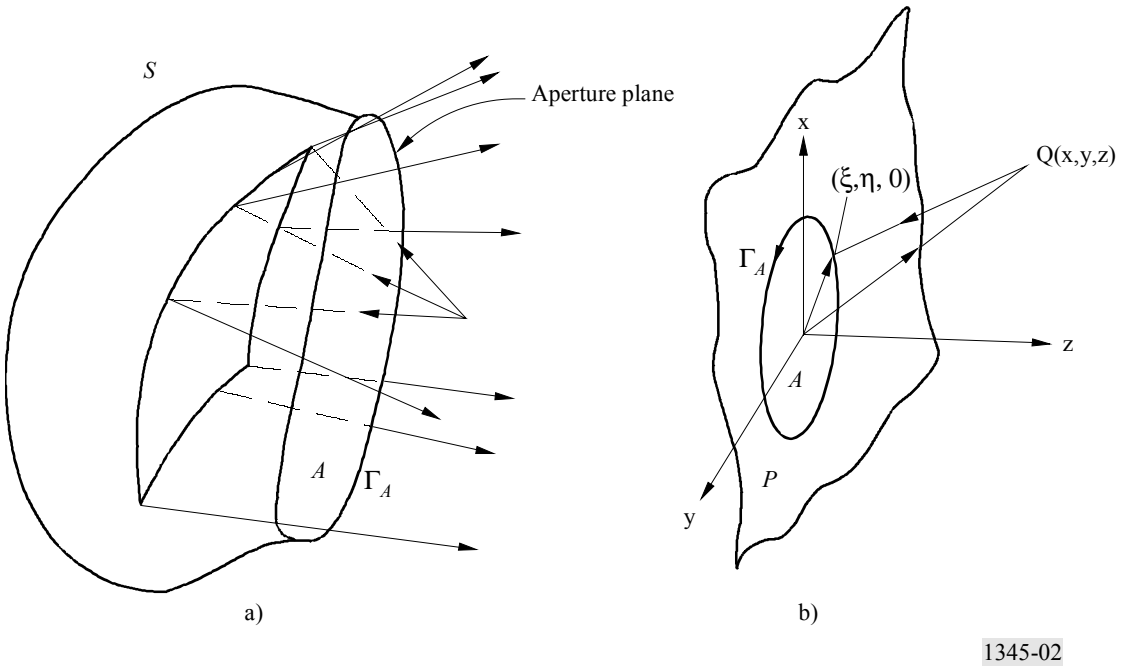

2.3 Scalar radiation integral/projected aperture method

The projected aperture method, (see Fig. 2b)), is essentially a simplification of the aperture field method discussed in the previous section. The surface *S* is taken to be made up of an infinite plane *P* (chosen on the radiating side of the reflector) closed at infinity by an infinite hemisphere on the source side, thereby enclosing the antenna. The field over the hemispherical sector vanishes (in view of the radiation condition) and the right hand side of equation (4) reduces to a surface integral over *P*. With some mathematical manipulation this can be transformed into a scalar radiation integral:

$$E_S = -\int_P \left(G\frac{\partial F}{\partial n} - F\frac{\partial G}{\partial n} \right) \mathrm{d}S \tag{5}$$

where *F* stands for any Cartesian component of the aperture electric field, and $\partial/\partial n$ is the normal derivative. Equation (5) can be written in a more usable form by taking *P* to coincide with the *x-y* plane as shown in Fig. 2b) with the sources confined to the sector $z < 0$. This gives the scattered field $E_S\ (x, y, z)$ at any arbitrary point, Q(x, y, z), as:

$$E_S(x,y,z) = \frac{1}{4\pi}\int_A F(\xi,\eta)\frac{\mathrm{e}^{-jkr}}{r}\left[\left(jk + \frac{1}{r}\right)(\mathbf{u}_z \bullet \mathbf{u}_r) + jk(\mathbf{u}_z \bullet \mathbf{u}_s)\right] \mathrm{d}\xi\, \mathrm{d}\eta \tag{6}$$

where *r* is the distance from the point (ξ, η, 0) on the aperture to the field point, Q(x, y, z), $\mathbf{u}_s$ is a unit vector normal to the wavefront at (ξ, η, 0), and $\mathbf{u}_r$ etc. are unit vectors along directions indicated by the corresponding subscripts. In equation (6), the integral has been truncated to a finite aperture $A \in P$ with the implicit assumption that $F(\xi, \eta) = 0$ over $P - A$. Sector *A* is the surface enclosed by the curve of intersection of the reflection shadow boundary with *P*.

In the far-field sector, along the direction given by (θ, φ), equation (6) simplifies further to:

$$E_S(\theta,\varphi) = \frac{j}{\lambda r}\mathrm{e}^{-jkr}\int_A F(\xi,\eta)\,\mathrm{e}^{jk \sin\theta(\xi\cos\varphi + \eta\sin\varphi)}\,\mathrm{d}\xi\,\mathrm{d}\eta \tag{7}$$

Equation (7) is the well-known scalar diffraction integral which expresses the far-field in terms of the tangential electric field over a planar aperture. In its derivation it is assumed that the phase of *F* varies little over *A* although this fact is often overlooked.

Equation (7) is widely used in the prediction of far-field patterns. The aperture field $F(\xi, \eta)$ is determined using geometrical optics in the sector of specularly reflected rays. The field truncates along the reflection shadow boundary Γ resulting in a discontinuity in $F(\xi, \eta)$ along Γ. This is, of course, not true in reality. Nevertheless, equation (7) has been widely used in the past and correctly predicts the main beam and near-in sidelobes.

The integral in equation (7) can be evaluated in explicit closed form for a large class of aperture fields. Since F is assumed zero outside A, the limits of integration can be set to $-\infty$ to ∞ without any loss of accuracy, whence it takes the form of a double Fourier integral. Fast numerical algorithms like the Fast Fourier Transform (FFT) can then be employed in its numerical evaluation.

This method is comparatively fast, and efficient codes that employ this technique are available for a wide variety of aperture type antennas. If the edge of the reflector forms a planar contour Γ, A can be chosen to be the surface circumscribed by Γ. In such cases, the radiation integral of equation (7) offers a distinct computational advantage over the physical optics approximation (discussed in the next section) since the integral in equation (7) is over a planar surface (unlike in the latter where suitable curvilinear coordinate systems need to be employed over curved reflectors). To a first order, this can predict deformities on the reflector surface that are large in terms of wavelength, typically those with minimum radii of curvature over five wavelengths in size for geometrical optics to be valid. Qualitative effects of aperture blockage can be accounted for by suitably tracking the rays. The effect of struts can be included in the analysis by a technique known as IFR (Induced Field Ratio) which is described in § 2.6 of this annex. As mentioned earlier, the projected aperture method can correctly predict only the main beam and first few sidelobes, and of necessity only the pattern in the forward hemisphere. However, it fails to predict the cross polar pattern with sufficient degree of accuracy, and it can be shown that the method gives symmetric patterns even in cases where there is asymmetry in the feed structure. In modern analysis, the projected aperture field method is always used in conjunction with GTD techniques (§ 2.5).

2.4 Physical optics

Physical Optics (PO) is essentially an approximation that relates the surface current on a conductor with the incident electromagnetic field. The scattered field $\mathbf{E}_s$ in an unbounded sector, due to a collection of electric and magnetic current sources $\mathbf{J}$ and $\mathbf{J}_m$ respectively, confined to within a finite volume V, is given by:

$$\mathbf{E}_s = -\frac{j}{\omega\varepsilon}\int_V \left[(\mathbf{J} \bullet \nabla)\nabla + k^2\mathbf{J} - j\omega\varepsilon\,\mathbf{J}_m \times \nabla\right] G\,\mathrm{d}v \tag{8}$$

If the source consists of simply an induced current density $\mathbf{J}_s$ on a perfectly conducting surface S, equation (8) transforms to a surface integral over S:

$$\mathbf{E}_s = -\frac{j}{\omega\varepsilon}\int_S \left[(\mathbf{J}_s \bullet \nabla)\nabla + k^2\mathbf{J}_s\right] G\,\mathrm{d}S \tag{9}$$

Equation (9) is exact and is valid at all points in space exterior to the source sector (on the actual sources the Green's function G has a singularity). If the surface current density $\mathbf{J}_s$ were known at every point on the reflector surface, the scattered field in both near and far-field zones could be determined from equation (9). Unfortunately $\mathbf{J}_s$ is not known, and its determination involves the solution of a complex boundary value problem. (In fact, method of moments is an attempt in this direction.)

Physical Optics is an approximation that expresses $\mathbf{J}_s$ at any point on the reflector in terms of the incident magnetic field intensity $\mathbf{H}_i$ at that point. Specifically, it is assumed that:

$$\mathbf{J}_s = 2\mathbf{u}_n \times \mathbf{H}_i \tag{10}$$

where $\mathbf{u}_n$ is the unit normal to S. This implies zero current on portions of the reflector surface not directly illuminated by the feed. Strictly, equation (10) is valid only for an infinite perfectly conducting plane. The actual current distribution is modified (from that given by equation (10)) by the finiteness of the reflector as well as by its curvature. If the radius of

curvature is large in terms of wavelength, equation (10) is very accurate except near the edges and in the shadow zone. Fringe currents along edge can be added to improve prediction, although this significantly increases computational complexity.

In the far-field sector, along the direction $\mathbf{u}_r$, equation (9) simplifies to

$$\mathbf{E}_s = -\frac{jk^2}{\omega\varepsilon}\frac{e^{-jkr}}{4\pi r}\left(\tilde{\mathbf{I}} - \mathbf{u}_r\mathbf{u}_r\right) \bullet \int_S \mathbf{J}_s(r')\exp(k\mathbf{r}' \bullet \mathbf{u}_r)\,dS \qquad (11)$$

where $\tilde{\mathbf{I}}$ is the unit dyadic. equation (11) is the standard far-field expression used in the PO approximation. In terms of CPU time and storage requirements, PO is comparable to the aperture field method. It is, however, generally more accurate than the latter and correctly predicts the main beam and close in sidelobes. It also gives a better prediction of the cross polar pattern. Smooth surface deformations can be easily modelled. In addition, the effect of struts, feed and other sub-systems can be added if the currents flowing on their surfaces (obtained by the PO expression of equation (10)) are taken into account but the interactions between various sources are not included, and as a result such predicted effects may have only a qualitative value. Physical optics is generally used in all cases except where the radiated field can be projected onto a planar aperture comparable in size to the reflector itself, in which case the projected aperture method is computationally significantly superior. As with the aperture field method, PO is now always used in tandem with high frequency diffraction techniques.

2.5 Geometrical theory of diffraction

Geometrical Theory of Diffraction (GTD) is a high-frequency technique suitable for the analysis of antennas that are large in terms of wavelength. It was originally formulated by Joseph Keller as an extension of Geometrical Optics (GO) to account for the non-zero fields in the shadow sector. This is accomplished by introducing a set of diffracted rays analogous to the reflected and transmitted rays of GO. Diffracted rays (Figs. 3 and 4) arise from edges, corners and from any other similar discontinuities in the surface curvature. Like GO, diffraction is assumed to be a strictly local phenomenon: this means the diffracted field depends only on the strength of the incident field at the point of diffraction, and on the local geometry of the diffracting wedge.

FIGURE 3

Diffracted ray come from a line of discontinuity

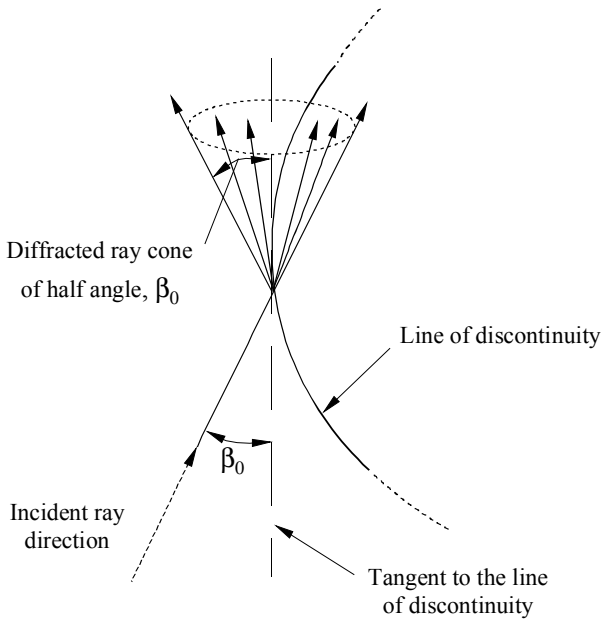

1345-03

FIGURE 4

Ray associated with reflection and diffraction from an impenetrable surface

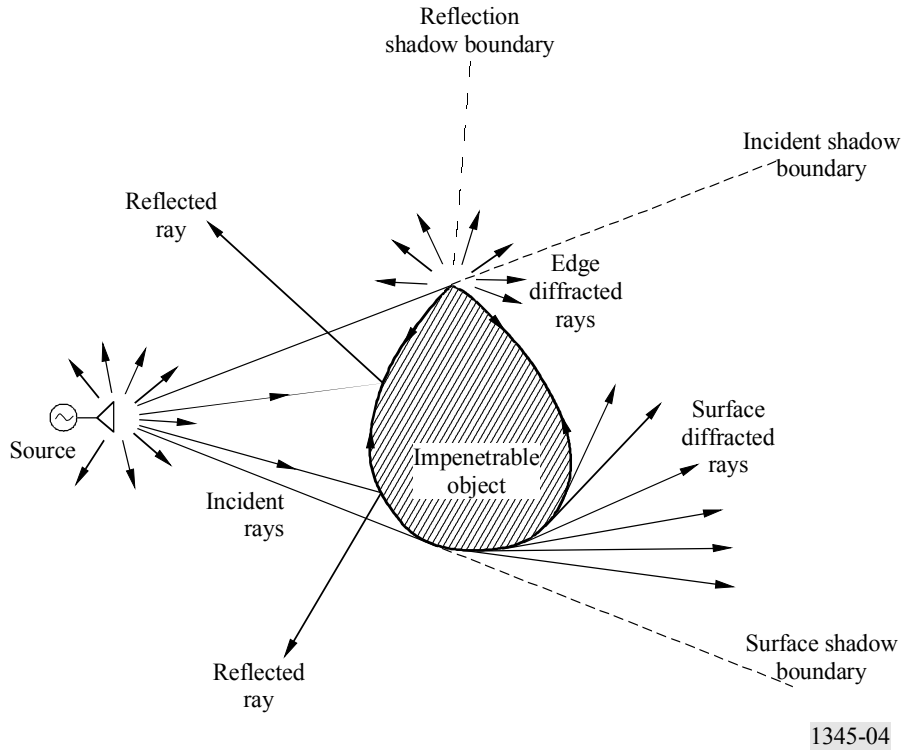

In GO, the reflected field is obtained by multiplying the incident field by a reflection coefficient. In a similar manner, the diffracted field is determined by multiplying the incident field by a diffraction coefficient; the latter is found as an asymptotic solution of a suitable canonical problem.

GTD along with its extensions is the most widely used high-frequency technique in reflector analysis.

According to GTD, the scattered field $\mathbf{E}_s$ at a point in space is given by:

$$\mathbf{E}_s = \mathbf{E}_r + \mathbf{E}_d \tag{12}$$

where $\mathbf{E}_r$ and $\mathbf{E}_d$ are the GO and GTD fields, respectively. The GO field is:

$$\mathbf{E}_r = \widetilde{\mathbf{R}}\mathbf{E}_i \, H \, \mathrm{e}^{-jks} \tag{13}$$

where $\widetilde{\mathbf{R}}$ is the dyadic reflection coefficient (made up of the Fresnel coefficients for reflection from an infinite dielectric planar interface), $\mathbf{E}_i$ is the incident field at the point of reflection Q_R, H is a divergence factor which depends on the principal radii of curvature of the incident wavefront, and those of the reflecting surface at Q_R, and s is the distance from Q_R to the field point. The diffracted field is, similarly:

$$\mathbf{E}_d = \widetilde{\mathbf{D}}\mathbf{E}_i \, L \, \mathrm{e}^{-jks} \tag{14}$$

where $\widetilde{\mathbf{D}}$ is the dyadic diffraction coefficient, and L is a similar divergence factor. Keller's expression for $\widetilde{\mathbf{D}}$, however, fails in the transition sectors close to the reflection and shadow boundaries, as well as at the caustics. To overcome this difficulty, "uniform" theories have been formulated that yield continuous functions across the transition sectors. These include the Uniform Geometrical Theory of Diffraction (UTD), and the Uniform Asymptotic Theory (UAT). Both

theories give values of $\tilde{\mathbf{D}}$ that have no singularity in the transition sectors, and have been successfully applied in far-field prediction for over two decades now. The diffraction coefficients contain Fresnel integrals that are easily evaluated, thus providing a fast and efficient algorithm for the analysis of large reflectors. In computation with GTD, most of the time is actually used in locating the points of reflection and diffraction on the reflector, given the source and field points. With multiple reflectors and complex geometrical shapes, this can sometimes be quite time consuming although not nearly as much as in evaluating double integrals over large surfaces.

Uniform theories, however, fail along caustics, defined as sectors where a family of rays converge to form focal points or focal lines. Such sectors can be analysed by the Equivalent Current Method (ECM), which works back from the GTD solution away from caustics to obtain an equivalent current that would produce identical fields there. This current is then used to extrapolate the field at the caustics. GTD, UTD, UAT and ECM all fail in sectors where GTD caustics and the transition sectors overlap. Such sectors can be treated by the Physical Theory of Diffraction (PTD), which is a systematic extension of the PO approach, just as GTD is an extension to GO. PTD formulates electric and magnetic edge currents from the GO fields tangential to the edge; to evaluate the diffracted field, it is necessary to integrate these currents along the length of the edge. In sectors where PTD and UTD/UAT both apply, it can be shown that the leading terms of the latter can be recovered from the PTD solution. However, application of PTD involves an additional integration along the edge, and numerical computations indicate that it does not improve accuracy over UTD/UAT techniques outside sectors where GTD caustics overlap GO shadow boundaries.

The main advantages of GO/UTD/UAT are that it renders itself to fast computation and that it can be used on arbitrarily shaped surfaces with arbitrary contours, provided the surfaces and contours have radii of curvature that are large in terms of wavelength. This means well-defined surface irregularities and surface deformations (caused, for example, by gravitational effects) can be treated by this method. Feeds and subreflectors can be accounted for through multiple reflections. In some cases imperfectly conducting surfaces and dielectric media can be included in the analysis. The GO/GTD method fails along caustics and alternative formalisms need to be invoked in such sectors.

2.6 Aperture blockage and strut effects

This section gives consideration to the modelling techniques for aperture blockage and strut effects.

The radio astronomy or space research antenna feed, the subreflector, if any, as well as the associated mechanical support structures and cable feeding may block some of the energy that would normally arrive at the antenna aperture. This problem is obviously much more important to axisymmetric systems than to offset arrangements. Nevertheless, these blockage problems reduce the performance of the antenna. The associated effects manifest as a reduction in gain, a significant increase in sidelobe levels (at least in certain directions) as well as deterioration in the polarization purity of the antenna system.

It is possible to include the blockage effects when we analyse the antenna pattern with any technique such as PO, aperture integration or GO/UTD.

Subreflector and feed blockage can usually be taken into account by considering the optical shadowing effects on the PO surface currents or aperture fields. This is usually adequate since it allows us to evaluate the drop in main beam gain and the changes in the near-in sidelobe levels. Equally well the radiation pattern due to the original understated illumination could be subtracted from the illumination that would exist hypothetically over the blocked portion of the structure. If a scheme is employed by which PO is switched to GO/UTD along certain directions then this subtraction approach could still be employed with the only difference that the “unobstructed” pattern will be calculated by the GO/UTD approach. As the main beam due to the “blocked illumination” is usually much wider than the main beam of the total antenna pattern, a PO or aperture integration can still be employed to calculate the blocked pattern over much wider angular

sectors than the range of validity of the corresponding methods for the core of the main reflector patterns. Effects due to struts can be also handed in a similar fashion, i.e. by considering the optical shadowing effects. This can be a successful approach provided that the strut cross-section is electrically large. If this is not true accurate predictions of strut effects are still possible with the aid of the Induced Field Ratio (IFR). The underlying philosophy behind the IFR concept is simple. The primary feed, after reflection from the main reflector, illuminates the struts and is then blocked; this illumination field has locally the character of a plane wave. The next step is to find the two dimensional (per length) "forward scattering" properties of an infinity long object having the same cross-section as the strut under plane wave illumination. Finally, the actual strut blockage field, and in particular the forward scattered field, can be calculated by scaling by the length and weight appropriate to the local illumination. The IFR concept allows the definition of two corresponding values for the two independent polarizations into which local incident plane waves can be decomposed; hence this methodology also allows the evaluation of polarization related effects due to strut scattering.

The IFR is a quantity which relates the actual forward strut scattered field to the strut blockage field under geometrical optics shadowing conditions. The formal definition of IFR for a cylindrical object under plane wave illumination states that it is a ratio between the forward scattered field to a hypothetical field radiated in the forward direction by a plane wave having a width equal to the optical shadow size of the geometrical cross section of the cylinder. The useful aspect of the IFR concept lies in the fact that the actual IFR quantity can be determined with analytical, numerical (Method of Moments, finite elements etc.) or even experimental techniques so as the strut effects can be predicted accurately. The analytical or numerical evolution of the IFR also permits, as an intermediate step, the determination of real or equivalent currents on the struts themselves. In principle, the full fan-shaped scattered pattern of the strut can therefore be calculated. In this case, the above process correctly includes the strut blockage and scattering effects over a large angular sector of the antenna pattern.

When the reflector surface is made of panels, interpanel gap diffraction can affect the radiation pattern as well as the boresight gain. These effects are naturally stronger as the frequency of operation increases and should be taken into account for antennas intended to be operational at millimetre wave frequencies. The concept of optical blockage is applicable if the gaps have an electrical large width. In the opposite case a Magnetic Current Induced Field Ratio (MIFR) can be defined, much along the same lines as the traditional IFR concept.

3 Recommendations

Most of the techniques outlined in § 2 are capable of predicting accurately the far-field patterns in their respective sectors of validity. In general, a complete characterization of the antenna pattern is best achieved by a suitable combination of various methods. The physical optics integration is the most widely used technique for large reflector analysis. It provides accurate results in the main beam sector and near-in sidelobes. Enhancing the PO solutions with GTD and its derivatives (UTD etc.) or with PTD provides full description of the antenna patterns in all directions including the wide angle illumination and back radiation.

The aperture field method plus GTD is used in some cases where S can be reduced to a plane. GTD based diffracted rays are added to cover a finite surface A where A is chosen such that F decays to a negligible value along its periphery. This leads to a smooth and continuous function F over the entire plane P and a planar integration quickly yields the pattern in the entire forward hemisphere. If A is considerably larger than the normal projection A' of the source antenna on P, then this method fails since the phase variation of F outside A' increases rapidly as we move further away from its boundary. If the rim of the reflector is planar, A can be chosen to cap the reflector.

Feed spillover past the reflector can be included by straightforward superposition of the fields, although GTD is also required to provide an accurate model close to the shadow boundary. Subreflector or feed blockage can be included as a shadow or projected shadow on the main reflector surface. The IFR technique can be used to estimate the strut

contributions. The IFR technique is limited to measured values or to the canonical problems that can be solved approximately or exactly and additional work may be required to establish the strut radiation patterns for a specific installation. However, general approximations can provide acceptable estimation to the levels of strut scattering which usually occurs at a significant angle from boresight (dependent upon the strut configuration) and this may be sufficient for most purposes. The Physical Optics integration technique can include the reflector deformation or feed/subreflector misalignments. The reflector profile can be determined experimentally by measurements or mechanical analysis. Microwave holography, theodolite based measurements and photogrammetry are diagnostic techniques that can also be used to assess the mechanical state of the reflector surface and associated systems such as feed and subreflector positioning, as described in Annex 2.

In many systems, the reflector is in the near-field of the feed or subreflector. This requires accurate evaluation of the near-field patterns of the feed or feed + subreflector combination. The Method of Moments (MoM) and hybrid MoM/GTD techniques may be suitable methods.

The combination of Physical Optics integration with UTD or PTD is the recommended analysis tool for predicting the radiation pattern of large reflector antennas. The “real” profile of the reflectors can be obtained by diagnostic techniques such as holography or photogrammetry.

Depending on the details of a particular installation, one should also take into account effects due to the environment in which the antenna operates. Radome effects, reflection from the ground and surrounding buildings are factors that should be taken into account. Due to the obvious complications of a composite antenna environment scenario, it is advisable to use the simplest possible technique. As such, a ray-based methodology is usually likely to be the only practical approach to evaluate the interaction of a large antenna with its immediate environment.

The recommendations are summarized in Fig. 5 and Table 2 below. The radiation pattern of a large reflector is divided into four sectors.

Sector I: Forward axial sector

Sector II: Far-out sidelobes

Sector III: Backlobes

Sector IV: Rear axial sector

The main mechanisms and recommended analysis techniques are given in Table 2.

TABLE 2

Mechanism and Analysis Techniques for Large Reflectors

	Main Mechanisms	Analysis Techniques
SECTOR I Forward axial sector	– Feed/subreflector performance – Overall antenna configuration – Reflector/feed alignment – Reflector distortions	PO
SECTOR II Far sidelobes	– Feed/subreflector performance – Overall antenna configuration – Reflector edge diffraction – Struts	GTD/UTD and IFR
SECTOR III Backlobes	– Reflector edge diffraction	GTD/UTD
SECTOR IV Rear axial sector	– Reflector edge illumination – Reflector edge geometry	Equivalent edge currents

FIGURE 5

Sectors for reflector analysis

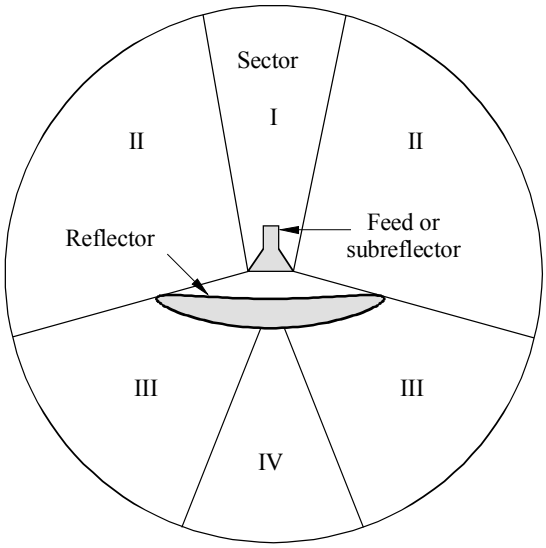

ANNEX 2

Analysis using experimental data

1 Introduction

Apart from relying in purely theoretical techniques, the radiation pattern of a radiotelescope antenna can be assessed when intermediate experimentally retrieved data are processed. The methods considered here involve experimental data associated with:

– Near-field probing

– Microwave Holography

– Theodolite based measurements

– Photogrammetry

Each of the techniques is described below. The most suitable technique for any application depends on the specific circumstances of each case and thus a general recommendation cannot be given.

2 Near-field measurements

The theoretical foundation of near-field measurements is based on the enclosing surface theorem as this is expressed by equation (4) in Annex 1. The only difference is that now symbol A is used to describe the full surface *S*. We can see that if the tangential fields over a surface enclosing an antenna are known, then the radiation pattern of the antenna can be found everywhere. Here however, rather than using a theoretical technique to evaluate the surface fields, direct measurements are involved.

Planar near-field probing can be used to evaluate the radiated fields over most of a hemisphere. On the other hand cylindrical and most importantly spherical near-field metrology can provide patterns for directions within most or all of the complete radiation sphere.

For these canonical geometries, the radiation pattern can be cast as an integration or summation of elemental plane wave components, cylindrical or spherical harmonics. Numerical algorithms exist which can carry out all the necessary arithmetic manipulation in a very efficient manner. However, the problems associated with the applicability of near-field metrology for the determination of the radiation pattern of a radio astronomy or space research antenna are due to the large amounts of near-field data required as well as the practical problems faced in order to acquire these data in a reliable way. The amount of near-field data required for an accurate pattern determination is defined by the necessary sampling interval. In the case of planar scanning this sampling interval should be $\frac{\lambda}{2}$ or less. For the case of a cylindrical scanning the sampling distance along the axis of the cylinder should be $\frac{\lambda}{2}$ or less whilst the angular sampling interval along the circular cross section should be $\lambda/(2R)$ in radians or less, where R is the radius of enclosing cylindrical surface. Similarly for a spherical near-field scanner the angular sampling intervals in azimuth and elevation should be at no more than $\lambda/(2R)$ radians.

From these sampling values it can be deduced that for common radio astronomy or space research antenna dimensions the amount of near-field data required is extremely large. In addition, there are significant mechanical, electrical and financial problems associated with devising suitable arrangements for the actual near-field data acquisition. These problems include the requirements for tight mechanical accuracies for the probe position when this moves over the large distances required to sample the field of the antenna. Also the RF source and metrology equipment should be sufficiently stable (or their variations should be reliably compensated) over the large time used for data acquisition. Environmental conditions can severely affect these near-field measurements which, due to practical considerations, have to be performed in open space.

For all these reasons a full near-field determination of a radio astronomy or space research antenna pattern cannot be a serious practical proposition. On the other hand, near-field probing can be used in order to evaluate the radiative properties of critical antenna subsystems such as the feed, compact feed-subreflector arrangements, or if used, beam waveguide feeding subsystems. These measured parameters can be used in a PO or GO + GTD like methodology to analyse the antenna performance.

3 Microwave holography

Microwave holography includes the measurement of the radiation performance of the antenna; extra complex measurements are performed from which the state of the telescope reflector profiles and alignment can be deduced. Holography can be used to identify the location and the magnitude of surface distortions. Additional information that can be retrieved from the holographic process can relate to possible feed displacement from the nominal focal position. The holographic process, achieves its goals when an accurate picture of the *phase variation* of the antenna's aperture field is established. Once this has been done, it is possible to employ ray tracing in order to interpret the aperture phase variation as surface profile information.

The holographic process starts with the recording of the antenna pattern not only in amplitude but also in phase. In order that reliable phase information can be recorded, a second (reference) antenna is usually employed which remains stationary throughout the measurement process. The pattern is recorded when a distant or close-by source is illuminating the antenna. In the latter case, the derived aperture phase distribution should be corrected for the quadratic type phase error resulting from the inadequate separation between antenna and source.

The actual sources used can be located in the terrestrial environment, can be geostationary satellite-borne, or even cosmic sources of microwave radiation. The latter two types are very useful for antenna holography as they allow the pattern measurement to be performed at elevation ranges similar to those used in the actual operation of the radio astronomy or space research antenna. Hence, the gravitational distortion effects will have much more representative values than in the case when a terrestrial illuminating source was employed. Holography based on space-borne sources offers the advantage over the use of cosmic sources in the sense that the measurement can be performed with a sufficiently large value of signal to noise ratio. It is, however, necessary to employ algorithms in order to compensate for the satellite movements throughout the measurement period, and special-to-type receivers are normally required.

Once the radiation pattern is recorded, the Fourier transform relationships are employed in order to derive the aperture field. Sampling theorem dictates that the radiation pattern should be recorded at discrete directions with a sampling interval δ_{UV} in the *U-V* space ($U = \sin\theta\cos\varphi$, $V = \sin\theta\sin\varphi$) such that:

$$\delta_{UV} \leq \lambda/D \tag{15}$$

where D is the diameter of the antenna. Fourier transform theory can be employed to prove that if an $N \times N$ measurement array is the *U-V* space is processed, then the aperture distribution can be recovered with pixel resolution having dimensions:

$$\delta_{XY} = \frac{\lambda}{N\delta_{UV}} \tag{16}$$

The recovered amplitude and phase value for a pixel represents the average values for the actual fields that exist in the corresponding area. This is the result of convolution type effects, due to the fact that only a truncated part of the total radiation pattern is recorded and subsequently processed. In this sense, holography can only record *local averages* and not point information for the antenna surface profile.

Polynomial fitting of the aperture phase information can recover deterministic errors such as gravitational and global thermal distortion and aberration due to axial and lateral displacement of the feed. If all these factors are subtracted then what remains can be attributed to a pseudo-random deformation of the surface profile. These random deformations can usually be attributed primarily to manufacturing errors, and if panels are used, to panel misalignment. In the latter case, these retrieved surface data can be used in order to improve the alignment state of the panels that form the reflector surface. In any case, the statistical properties of the antenna surface are usually described by σ which is the r.m.s. value of the surface deviation from a specified (usually parabolic) reflector profile. The value of σ that can be unambiguously determined from the holographic process depends on a number of factors including the operating wavelength, the signal to noise ratio, the extent of the measured pattern record, phase instabilities on the receiving systems etc. Practical measurements have indicated that the highest achievable D/σ values that can be reliably measured are of the order of 250 000.

Once holographic information for the antenna is retrieved it is possible to provide analytical expressions for the reflector surface using spline interpolation functions, zernike polynomials etc. This is primarily the value of holography as a pattern prediction tool. The analytical surface description can now be used in conjunction with any technique such as PO, PO + PTD, or GO + GTD to provide radiation pattern data over angular sectors not covered in the original holographic data acquisition or for frequencies other than the one used in the holographic process. Due to the convolution phenomena explained earlier, certain information on the surface profile variation is inevitably lost. This means that the employed surface description may not be entirely correct. Hence some ambiguity may exist as far as the accuracy of the predicted far out sidelobe level is concerned. However, this situation may not be as bad since the far out sidelobes are also strongly influenced by the accuracy with which the reflector rim geometry and associated illumination is reproduced in the theoretical model.

The holographic approach may not however be entirely successful in providing surface profile information when a multireflector antenna is considered. In this case, it is not straightforward to correctly and unambiguously associate retrieved aperture phase information with deterministic or random profile errors for the main reflector or the subreflector(s).

As it can be seen from the above, microwave holography is not normally needed if the only requirement is to assess the antenna RF performance rather than to also identify the profile errors causing performance degradation. However, the technique can be used to measure the antenna at an intermediate range and derive the far-field.

4 Theodolite based measurements

Measurements using theodolites, as well as the photogrammetry methods which will be discussed later, are optically based approaches which utilises the geometrical nature of optical propagation in order to establish the geometrical coordinates of selected points (targets). These targets can be set on the surface of the main reflector, the subreflector, the backing structure, the struts or even on the primary feed of the antenna.

The theodolite is an instrument that basically measures two angles, one elevation and one azimuth, as it aims at the target position. There are basically two variants of theodolite measurements that can be made:

– The theodolite and tape method

– The multi-theodolite station, triangulation

In the theodolite and tape method the coordinates of a point are expressed in a coordinate system associated with the theodolite. The instrument itself basically offers the two polar angles of a target. The radial distance of the target from a theodolite reference point can be measured with either a steel tape or more accurately with a laser rangefinder.

The theodolite and tape system is assumed to be calibrated prior to the actual start of the measurements. Also, there appears to be a potential problem at non-zenith locations as gravity disturbs the optical instrument as it tilts (as it will if mounted on the reflector) and so it must be specially designed.

In multi-theodolite station triangulation, the targets are surveyed by two or more (usually between 2 and 4) instruments placed at different locations in front of the antenna. At this stage only angular measurements are recorded. It is possible to set up a universal coordinate system so that the rectangular coordinates of every target can be expressed unambiguously; the precise location of every theodolite station should therefore be accurately known in advance. This is the calibration phase (which is always the first task during a theodolite based measurements) and essentially consists of surveying known points, such as end points of a reference marker, bars, etc.

The measurement accuracy of theodolite systems is of course affected by the basic accuracy of the instrument. Nowadays, highly accurate digital theodolites can offer significantly reduced errors of about 0.5 arc sec. This means that the final accuracy of the theodolite measurement will be more dominated by the accuracy of the calibration process and less by the basic accuracy of the measurement itself. The accuracies experience in actual measurements expressed on the ratio of D/σ explained earlier is of the order of 120 000 for two theodolite station and 250 000 for four theodolite stations.

5 Close range photogrammetry

Photogrammetry is a process of obtaining reliable geometrical information for an object by measuring its photographic images. Again a number of target points are defined on the antenna structure. Using specialized photogrammetric cameras, the antenna is photographed from different directions such that the given targets will appear in more than one photograph. The coordinates x,y of a target image expressed in a photographic plate coordinate system are determined. Using the "projective equations" one can relate the image coordinates of a given target to its true 3-D coordinates associated with a universal system. The set of projective equations for all targets on the antenna, and for every photograph taken, forms the basis of the photogrammetric triangulation process.

The projective equations for every target are dependent on a set of parameters (projective parameters) which are constant for every individual photograph. The determination of these constants is the goal of the calibration phase. Calibration can be performed along similar lines as those used in theodolite based measurements, i.e. surveying a number of control points. However, the ability of photogrammetry to record a number of targets within a single photograph can enable an alternative calibrating procedure which runs concurrently with the actual target position determination. In essence, the possibility of having a given target recorded in a number of photographs leads to an over-determined system which can be solved by least square methods. This approach yields the projective parameters through a reduced set of equations. The coordinates of the target points can be deduced afterwards. Such an approach is called the "bundle method".

There is a similarity between multi-theodolite system method and photogrammetry as both methods utilise the triangulation method for establishing the target coordinates. There is however, an important difference in the sense that in photogrammetry there is no need to know the precise position of the instrument station. This point can be retrieved from the measurements as the bundle of rays representing the targets imaged in a photograph are always assumed to be stigmatic at the reference station position.

The accuracy of photogrammetry increases as the number of photographs increase and photogrammetry makes it easier to survey more points and at more different locations than in the case of theodolite measurements. Photogrammetry is also very "quick", which is good if time variant parameters are present, as they usually are. (Mechanical measurements on large antennas often have to be performed at night with good cloud cover for constant temperature.) These advantages combined with the above mentioned powerful calibration procedure makes photogrammetry a more accurate coordinate determination procedure than when theodolites are employed. D/σ accuracies of 250 000 are routinely available from photogrammetry with figs. such as 500 000 or even 1 000 000 entirely feasible from a careful photogrammetric survey of large antenna structure. However, since the antenna is usually tilted in elevation to almost horizontal during the measurements, unrepresentative gravitational deformations may be introduced.

Since surveying a large number of points is possible with photogrammetry, a better expression of the antenna main or subreflector surface can be found than by other measurement techniques. Processing this data with any technique such as PO or GO + GTD can yield a good estimate for the radiation pattern over an extended angular sector.

ANNEX 3

Example results of computer modelling

1 Introduction

A commercially available software package[1] has been used to model the antenna gain patterns of a large radio astronomy antenna. The results illustrate the effect of various parameters on the model's predictions and the significance of various mechanical features.

2 Model methodology

The model uses a combination of the Physical Optics (PO) and Geometrical Theory of Diffraction (GTD) approaches.

For the PO calculations, the surface of the reflector is divided into a grid of surface elements. The radiated field is found by integration of the surface currents at each point on the grid. To simulate the effect of aperture blockage, the surface currents are set to zero in the shadow of the feed on the reflector surface.

The GTD approach follows three steps:

1. Selection of significant rays
2. Ray tracing
3. Field calculation

A simple caustic correction procedure is applied which smoothes the diffracted field for angles close to the caustic direction. It cannot however accurately predict the field close to the caustic in the boresight direction.

---

[1] "GRASPC" from TICRA (Denmark).

The GTD method, in general, requires less computation time than the PO approach. Therefore, GTD is used for all angles except where GTD is inaccurate. Due to the caustic on boresight, the PO method is used for angles in this sector.

Struts are treated by a method based on the Induced Field Ratio concept. To simplify the method, it is assumed that the strut is circular and the field contribution from the strut is limited to far-field analysis only.

Random surface distortions can be imposed on the surface of the main reflector. The distortions are correlated over a distance consistent with the size of the individual panels of the reflector surface.

3 Antenna mechanical parameters

The Lovell Mk1A radio astronomy antenna, located at Jodrell Bank in the UK was modelled. The major parameters of this antenna are shown in Table 3.

4 Model results

The antenna was modelled at 150 MHz and at 5 000 MHz. It was modelled in the far-field, both with and without struts. The effects of varying the observation distance within the near-field were examined and the effects of surface distortions were examined.

The antenna was also modelled at the 1 420 MHz in order to compare the results with measured data taken at the same frequency.

All the results are for the Mk 1A antenna assumed to be transmitting with circular polarization. The receiver is assumed to be using vertical polarization. All patterns are for the azimuth plane, with the antenna pointing at 0° elevation.

TABLE 3

Parameters of Mk 1A radio astronomy telescope

Diameter	76.2 m, circular aperture
Focal Length	22.9 m, primary focus
Frequency Range	150-5 000 MHz
Support struts	The Mk 1A has a central pylon supporting the feed, this has been modelled as four individual struts, diameter 0.2 m
Feed housing	3.8 m diameter
Feed gain pattern	Parabolic, 13 dB below maximum at 59°
Surface distortions	6 mm r.m.s. (25 mm peak-peak)
Surface distortion correlation distance	2.8 m

4.1 Far-field and near-field at 150 MHz

Fig. 6 shows the gain pattern at 150 MHz, with surface distortions included and with no struts. The PO method was used within 7.06° of boresight, and the GTD method at other angles. The 4 plots show the changing gain pattern as the observation point moves from far-field to successively shorter near-field distances. At this frequency, the far-field distance is 5.8 km.

It can be seen that the far-field pattern and the near-field pattern at 1 000 m are almost identical. For distances of 100 m and 50 m, the width of the main lobe increases and the maximum gain decreases. Beyond ±130°, there is little change in the level of the side-lobe envelope. At these angles the dominant rays are the edge diffracted rays.

FIGURE 6

Mk 1A at 5000 MHz without struts, far-field and near field

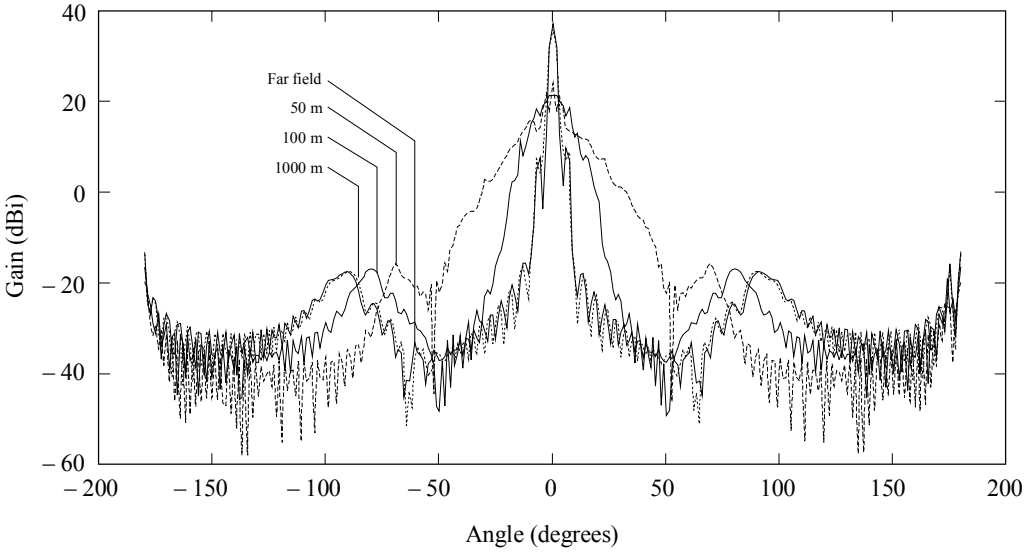

4.2 Far-field at 5 000 MHz, with and without struts

Fig. 7 shows the far-field gain pattern of the Mk 1A at 5 000 MHz. Random surface distortions are included. The PO method was used within 0.21° of boresight, and the GTD method at other angles. One plot shows the pattern with no struts, the other has struts included. The reference radiation pattern from Recommendation ITU-R SA.509 is included.

Without struts, the effect of spillover (radiation directly to or from the feed) is visible from the peaks at about ±100°. When struts are included, the high level of strut scattering predicted by the model tends to mask the spillover effects. With struts included, the gain pattern just exceeds the reference radiation pattern for angles less than 100° from boresight.

FIGURE 7

Far-field of Mk 1A at 5000 MHz, with and without struts

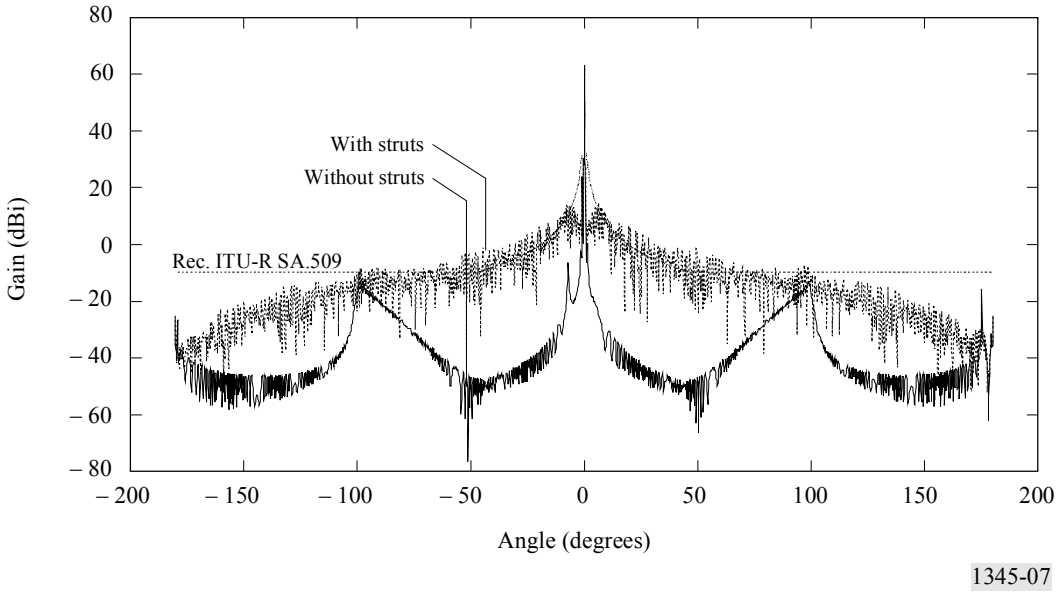

4.3 Far-field at 5 000 MHz, with and without surface distortions

Fig. 8 shows the effect of using a different random number seed for the distribution of random surface deviations. Three far-field plots are shown for the MK 1A at 5 000 MHz. They are separated by 50 dB for clarity. One gives the predicted pattern with no surface distortion, the others show the effect of different random distributions. The PO method was used within 0.21° of boresight, and the GTD method at other angles.

One can see that the surface distortions produce "spikes" near the main beam. The "spikes" are about 10 dB higher than the level with no surface distortion. Beyond about 10° from boresight, surface distortions appear to have little effect. If strut scattering were included (as indicated by Fig. 7), the "spikes" close to boresight would be masked.

4.4 Far-field and near-field at 5 000 MHz, without struts

Fig. 9 shows the effect of viewing the antenna in the near-field. The plots are for the Mk 1A at 5 000 MHz with surface distortions, viewed from the far-field and at 3 different near-field distances. The PO method was used within 0.21° of boresight, and the GTD method at other angles. The plots are separated by 70 dB for clarity.

The prediction for a near-field distance of 10 km is almost identical to the far-field plot. At the 1 km observation distance the main beam becomes wider and the maximum gain is lowered. At 100 m the main beam is wider still and maximum gain is lowered again. Beyond ±50° there is little difference in the level of the side-lobe gain. The peaks at around 100° are due to spillover from the feed. The angle at which the spillover peaks occurs is seen to change as the observation distance is shortened. This is because the centre of the coordinate system is at the centre of the main reflector and the angle between boresight and the edge of the main reflector changes with distance.

FIGURE 8

Far-field at 5000 MHz, with and without surface distortion

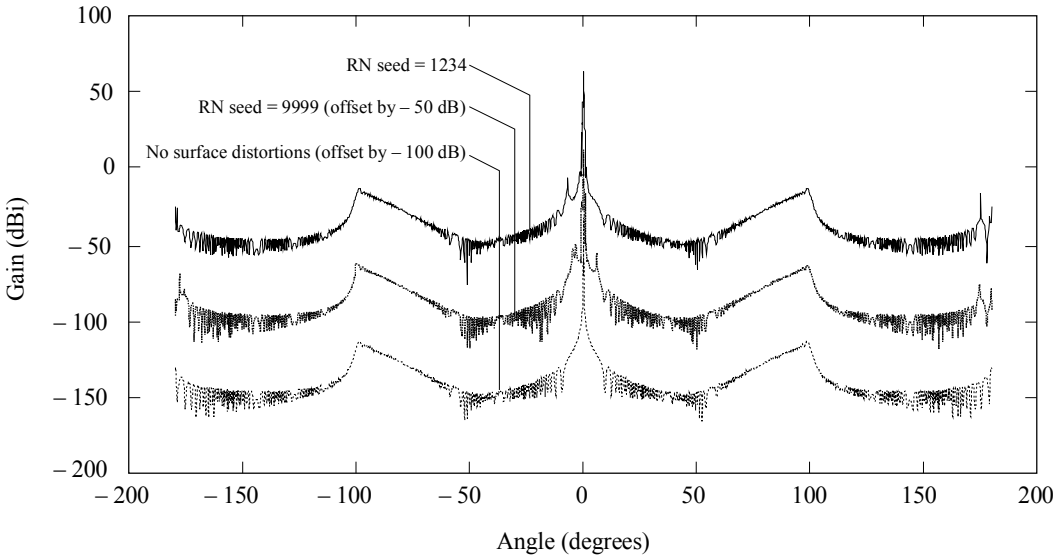

FIGURE 9

Mk 1A at 5000 MHz without struts, far-field and near field

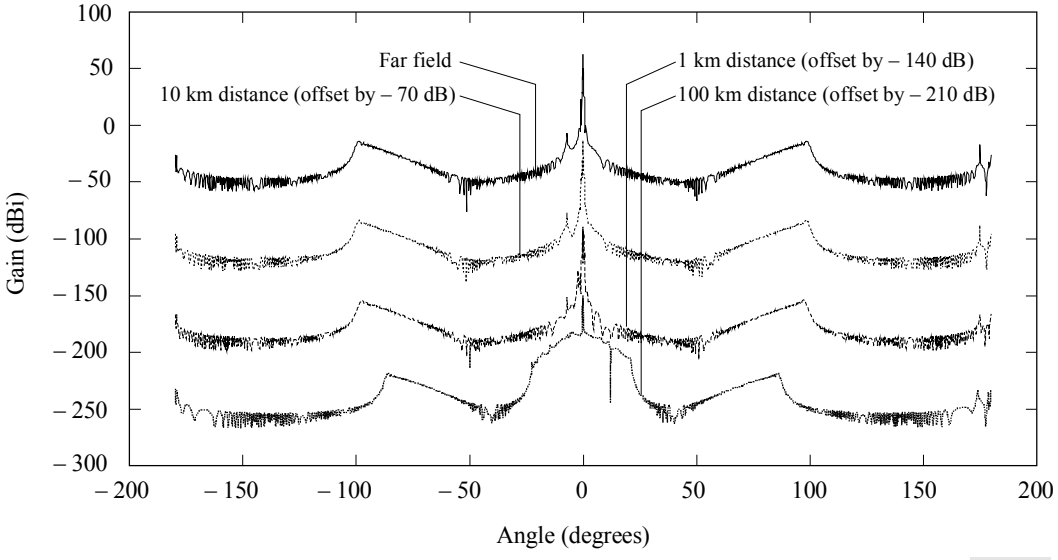

4.5 Comparison of measured pattern with model prediction

Fig. 10a) shows a far-field prediction for the Mk 1A at 1420 MHz. The gain is relative to the maximum gain of 57 dBi. Fig. 10b) shows the measured gain of the Mk 1A at the same frequency. The peak in the measured signal at around 95° is due to spillover.

The model appears to underestimate the level of the side-lobes close to the main beam (to about 15°), and the high level of spillover. For the sidelobe level between 15° and 80°, there are a limited number of samples but the predicted level appears approximately to be correct.

FIGURE 10

Mk 1A at 1420 MHz: a) far-field model prediction (top), b) measured gain (bottom)

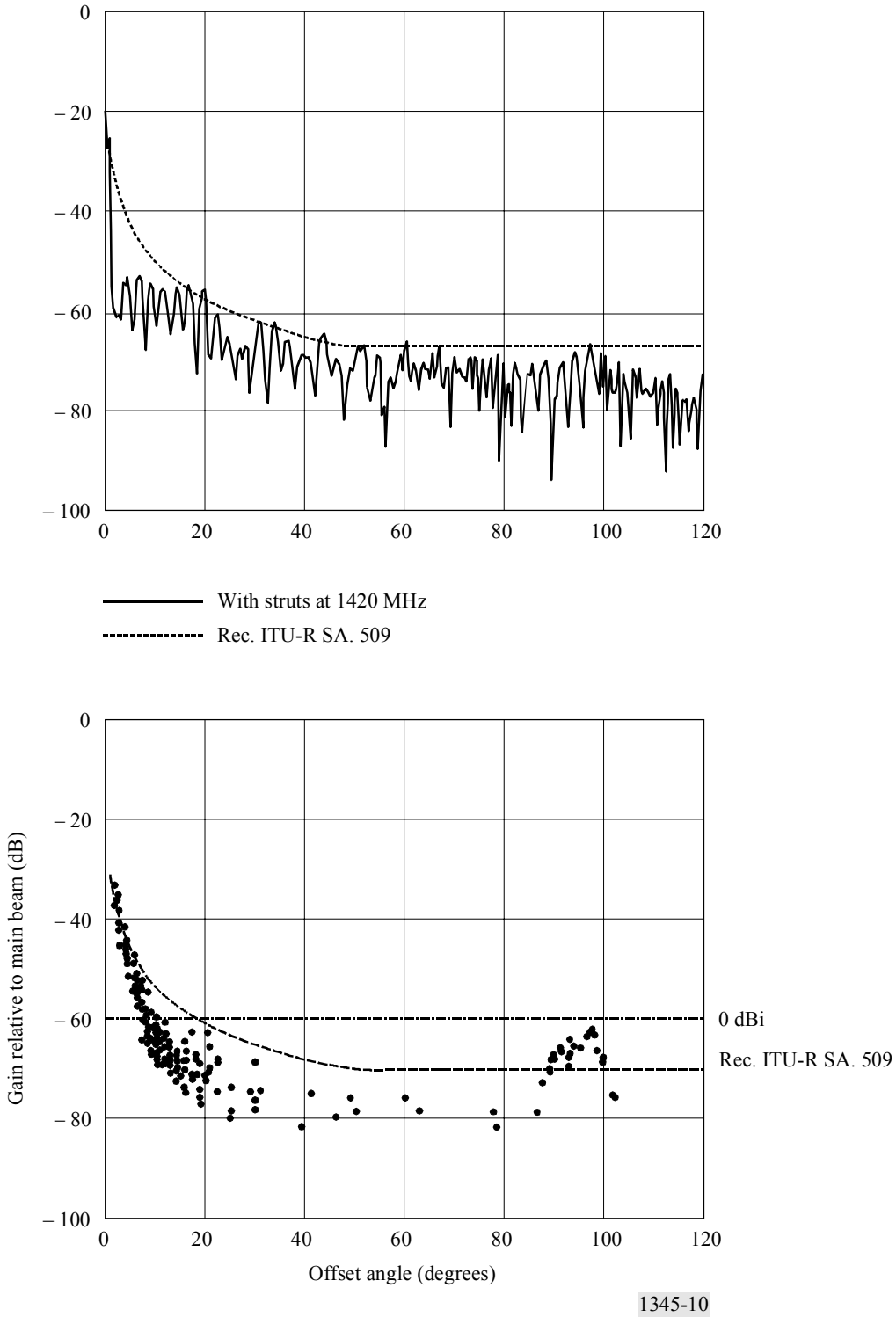

5 Conclusions

The importance of the feed support struts, feed gain pattern and surface distortions to the modelling of the side-lobe gain pattern of large antennas has been considered.

5.1 Feed support struts

For a wide range of angles, the sidelobe level is dominated by scattering from the struts. Within this sector the accuracy of the treatment of struts is therefore the dominant factor.

5.2 Feed gain pattern

At certain angles of view, spillover (radiation direct from the feed) can be a dominant factor. For many antennas, spillover produces the highest peak in the far out sidelobe envelope. In the case of the Mk 1A, spillover is dominant between approximately 90° and 100°. Thus knowledge of the feed horn gain pattern, particularly at angles near the spillover angle, is an important parameter.

5.3 Surface distortions

The distortions to the surface of the reflector can cause an increase in the level of the near-in sidelobes. The effect can be significant when the wavelength is of the same order as the size of the surface errors.